Supporting Information

Meissirel et al. 10.1073/pnas.1100341108

SI Materials and Methods

Animals. Swiss or C57BL/6J [postnatal days 5–6 (P5–P6)] mice were used for granule cell (GC) purification. Wistar rat pups (P8) were also used for immunostainings. All animals were treated according to the guidelines approved by the French Ethical Committee (agreement no. 693880201) and the Animal Care Committee of the University of Leuven, Leuven, Belgium.

GC Purification and Chemotaxis Assay. GCs were purified as described in ref. 3. Purified GCs were resuspended in serum-free DMEM supplemented with N2 and B27 (Gibco; Invitrogen). The in vitro migration of GCs was assessed by using polyvinyl carbonate-free membranes (8-μm pore size), coated with laminin (20 μg/mL; Sigma), in modified Boyden chambers as described (4). Briefly, 100 μL of a solution containing 1×10^5 cells in serum-free DMEM was placed in the upper chamber. VEGF (50 ng/mL), D-2-amino-5-phosphono-valerate (D-APV, 100 μM; Tocris) or NMDA (10 μM) was added alone or in combination in serum-free DMEM (supplemented with N2 and B27) in the lower or upper chamber, respectively. After overnight incubation, the upper surface of the membranes was scraped free of cells and debris and membranes were rinsed, fixed, stained for βIII-tubulin, and counterstained with DAPI. GCs that had migrated through the pores and adhered to the membrane were analyzed by high-power fluorescent microscopy and counted in 30 nonadjacent high-power fields. Experiments were performed in duplicate. GCs at the lower side of the filter in treated conditions were expressed as a percentage of those in control conditions. Statistical significance was analyzed by one-way ANOVA followed by post hoc testing with correction of the *P* values for the number of tests performed.

Immunohistochemistry. ***Cerebellar slices.*** P10 mice were injected i.p. with BrdU (50 mg/kg of body weight); 3 h later, cerebellar slices (350 μm) were made and cultured for 4 d in vitro (DIV). Subsequently, slices were fixed in 2% PFA/30% sucrose for 2 h at room temperature before BrdU immunostaining with an anti-BrdU (OBT 0030S Harlan; Oxford Biotechnology) antibody, followed by incubation with an Alexa Fluor 568-conjugated secondary antibody (Molecular Probes).

Isolated GCs. Purified GCs plated on poly-L-lysine and laminin-coated coverslips were fixed for 4 min with 4% PFA and 4% sucrose in PBS without detergent to avoid permeabilization, washed with PBS, and then blocked with 1% BSA in PBS for 1 h at room temperature. Surface receptors were stained overnight at 4 °C in 1% BSA in PBS with antibodies recognizing extracellular epitopes of the corresponding proteins (anti-NR2B, 1/12.5; Zymed Laboratories; and anti-Flk1, 1/25, clone AF644; R&D Systems). Coverslips were subsequently incubated with fluorescently conjugated secondary antibodies: Alexa Fluor 568 for Flk1, and Alexa Fluor 633 for NR2B. After staining, cells were fixed with 4% PFA, and permeabilized with 0.1% Triton X-100 in PBS. After blocking, they were stained with anti-β-III tubulin (1/200; Sigma) and Alexa Fluor 488. Finally, stained GCs were counterstained with DAPI by mounting the coverslips with ProLong Gold plus DAPI (Invitrogen).

Ex Vivo Cerebellar Electroporation. Cerebella dissected from P6, P8, or P10 WT pups were injected with 4–8 μL of the DNA of interest (3 μg/μL; EndoFree, GFP-expression vector in 5:1 ratio) into the superficial layers of the cerebellum. The following shRNAi constructs were used for Flk1 ($Flk1^{KD}$) and for the control ($Flk1^{Ctl}$): pENTR-U6-shFlk-KD: 5′-CACCGGAGAAATCGCTCAGTGATGTTCTCTTGAAACATCACTGAGCGATTTCTCC-3′; and pENTR-U6-shFlk-Ctl: 5′-CACCGGAGTATCCCCCGACACATCTTCTCTTGAAAGATGTGTCG-GGGGATACTCC-3′. The DNA of interest was diluted in PBS together with 0.2% Fast Green (Sigma). The cerebellum was subjected to five electric pulses of 85 V, 50 ms, and a 1.0-s delay between pulses by using 10-mm electrodes connected to a square pulse ECM 830 ElectroSquarePorator (BTX Harvard Apparatus). Meninges were removed, and 350-μm slices were made with a tissue chopper (McIllwain). Slices were incubated in Millicells (Millipore) at 35 °C, 5% CO_2 and in medium containing 94.5% basal medium Eagle (Gibco), 1% glucose, 0.5% BSA, 1% penicillin/streptavidin (Gibco), and 1% supplement insulin/transferrin/selenium (Sigma).

Culture and Treatment of Cerebellar Slices. Cerebellar slices were cultured for 3–4 d as described previously (5). Slices for GC migration analysis were treated with anti-Flk1 blocking antibody (αFlk1; 30 μg/mL), D-APV (25 μM), or a combination of αFlk1 (30 μg/mL) plus D-APV (25 μM) by adding them to the culture medium. Half of the medium was refreshed every day with new inhibitors.

Analysis of Flk1 and NR2B Coclusters. Purified GCs (1 DIV) were stimulated with VEGF (50 ng/mL) for 10 min, fixed in non-permeabilized conditions, and immunostained for Flk1, NR2B, and βIII-tubulin as described above. Imaging of GCs was performed with an LSM 710 laser scanning microscope (Zeiss) equipped with 34 spectral reflection/fluorescence detection channels and five laser lines (458, 488, 514, 543, and 633 nm). GCs were imaged with a Plan-Apochromat 100×/1.40 oil differential interference contrast M27 objective. The laser scanning microscopy imaging software ZEN (version 2009) was used for digital acquisition and processing of the images. An average of 4 frames per image and a scan speed of 7 frames per s were used for acquisition. The indicated laser beams were used for DAPI (405 nm), Flk1 (543 nm), NR2B (633 nm), and βIII-tubulin (488 nm). Stacks of confocal optical slices were collected digitally, and 3D reconstructions of image data were generated with the ZEN (version 2009) software package. Analysis of Flk1 and NR2B coclusters was performed by using the image analysis software package Imaris (version 6.3.1) (Fig. S5). Clusters were detected in the maximum projection of 3D confocal *z*-stack images by using a customized algorithm in which, for each fluorescent channel, a cluster was defined by an estimated diameter (between 0.04 and 0.1 μm) and by a threshold of mean fluorescence intensity (after subtraction of the background signal). Coclusters were identified by generating a colocalization channel and applying the same fluorescence intensity threshold and estimated diameter used for identifying single clusters (Fig. S5). The statistical analysis of the number of clusters and coclusters per cell was performed by calculating the estimated marginal mean and the SEM of the absolute values by a general linear model (univariate ANOVA) while correcting for the experiment ($n = 3$ independent experiments). We used SPSS 16.0 to perform all statistical analyses.

Electrophysiological Recordings. Whole-cell patch–clamp recordings were performed on acute parasagittal cerebellar slices from P8 to P9 C57BL6 mice and on organotypic parasagittal cerebellar slices from P6 C57BL6 mice cultured for 3 DIV. Briefly,

cerebella were removed, placed in cooled saline (2–4 °C), and sectioned with a Vibratome (VT1000S; Leica) into 250-μm-thick slices (6). The saline solution used for slicing contained 85 mM NaCl, 26 mM $NaHCO_3$, 2.5 mM KCl, 1.25 mM NaH_2PO_4, 0.5 mM $CaCl_2$, 4 mM $MgCl_2$, 25 mM glucose, and 75 mM sucrose. Slices were maintained at room temperature for up to 6 h in the incubation solution equilibrated with 95% O_2 and 5% CO_2. Whole-cell patch–clamp recordings from GCs in the lower external GC layer (EGL) were performed in acute or electroporated slices with an Axopatch 200A amplifier (Axon Instruments) under visual control using an upright microscope equipped with infrared light and fluorescence (BX50WI; Olympus). GCs in the lower EGL were identified visually under Nomarski differential interference contrast optics and, for $EGFP^+$ GCs, with a filter set for a 488 fluorophore. Internal recording solution contained 120 mM Cs-gluconate, 1 mM EGTA, 2 mM $MgCl_2$, 10 mM phosphocreatine, 0.1 mM $CaCl_2$, 4 mM Na-ATP, 0.4 mM GTP, and 10 mM Hepes (300 mOsm at pH 7.2). Neurobiotin (0.5–1%) was routinely added to the internal recording solution to allow post hoc morphological identification of the recorded cells. The typical pipette resistance was ∼8 MΩ for GCs. GCs were characterized electrophysiologically by their absence of action potentials and synaptic events as well as by their high input resistance (5.9 ± 0.8 GΩ) and small cell capacitance (7). The perfusion solution contained 124 mM NaCl, 26 mM $NaHCO_3$, 2.5 mM KCl, 1.25 mM NaH_2PO_4, 2.5 mM $CaCl_2$, and 10 mM glucose with 0.5 μM strychnine hydrochloride (Sigma) and 100 μM glycine (Sigma). To record NMDAR-mediated currents in GCs, 10, 25, or 50 μM NMDA (Tocris) was added to the perfusion solution, and VEGF (150 ng/mL; R&D Systems) was applied locally with a 2-μm-diameter micropipette above the recorded GC (∼15 μm) by pressure (0.5 bar; Picospritzer II) during 50 ms at a frequency from 0.1 to 0.5 Hz. VEGF was topically applied to minimize possible indirect effects. Control experiments with topical saline or PBS application revealed that the mechanical stimulus associated with this local administration route did not evoke any NMDAR-current (data not shown). NMDAR-mediated responses were blocked by using the selective NMDAR antagonist D-APV (Tocris) at 50 μM. The small Src-family kinase (SFK) inhibitor PP1 (10 μM) or its inactive homolog PP3 (10 μM) was applied through the patch pipette to block SFK directly in the recorded cell. GCs were recorded in voltage–clamp mode, and a ramp of potential from −80 to +20 mV or −60 to +40 mV (100 $mV{\cdot}s^{-1}$) was applied. The current amplitudes were plotted against voltage, and the data were fitted by linear regression to generate a slope conductance and reversal potential. Online and offline data analysis were carried out with Acquis1 (G. Sadoc, Centre National de la Recherche Scientifique, French National Innovation Support Agency, France). A paired *t* test was applied for statistical analysis of electrophysiological experiments.

Transfection of HEK-293 Cells. HEK-293 cells were maintained in DMEM supplemented with 10% FBS and transfected by using the calcium phosphate method or Lipofectamine (Invitrogen). The following plasmids were used for transfection: Flk1, NR1, NR2B-GFP (termed NR2B), shRNAi for Flk1 ($Flk1^{KD}$), control shRNAi ($Flk1^{Ctl}$), NR2BTM, Src^{WT}, and Src^{DN} (mutations Y295R and Y527F). For HEK-293 cells expressing recombinant NMDARs, ketamine (500 μM) was included in the media 16 h after transfection and washed out before VEGF stimulation. For the phosphorylation experiments, cells were starved 1 d after transfection in 0.1% serum containing medium with ketamine for 16–20 h. Afterward, GCs and HEK-293 cells were stimulated with VEGF (50 ng/mL) for 5 or 15 min, as indicated. For testing the effect of a combined NMDA plus VEGF stimulus (Fig. S2), cells were stimulated with NMDA (3 μM) or control medium for 10 min and subsequently incubated with VEGF (50 ng/mL) for 30 min in the presence of NMDA or control medium.

Calcium Imaging. GCs were exposed to NMDA (30 μM) for 7 min through a perfusion system, washed in Hepes-buffered saline solution (HBSS) for 10 min with a perfusion system, and then incubated (no perfusion) with VEGF (10 ng/mL) for 15 min. Thereafter, a second NMDA [± D-APV (100 μM)] pulse of 7 min was given. IgG (10 μg/mL) and αFlk1 (10 μg/mL) were preincubated for 15 min (no perfusion) before adding VEGF (10 ng/mL) and incubating the cells for 15 min (no perfusion). GCs were incubated with PTK787 (PTK; 3 μM; LCL Laboratories) or its control vehicle for 5 min (no perfusion), then washed (with HBSS) for 5 min with perfusion and incubated with VEGF (10 ng/mL) for 15 min with no perfusion before the second NMDA pulse. GCs were incubated with PP1 (3 μM) and PP3 (3 μM) for 10 min (no perfusion), washed (in HBSS) for 5 min with perfusion, and subsequently exposed to VEGF (10 ng/mL) for 15 min with no perfusion. HEK-293 cells were exposed to NMDA (30 μM) for 5 min with perfusion, washed (with HBSS) for 10 min with perfusion, treated with VEGF (10 ng/mL) for 15 min with no perfusion, and thereafter exposed to a second pulse of NMDA (30 μM) for 5 min with perfusion. Fura-2 (excitation: 340 and 380 nm; emission: 510 nm) ratio images were acquired with a CCD camera (Princeton Instrument) and digitized (256 × 512 pixels) with MetaFluor 6.2r6 software (Universal Imaging Corporation). ΔCa^{2+} was calculated as the difference between the maximum Ca^{2+} influx ($[Ca^{2+}]_i$) during NMDA stimulation and basal $[Ca^{2+}]_i$.

Immunoprecipitation and Immunoblotting. GCs or transfected HEK-293 cells, stimulated with VEGF (50 ng/mL) for 15 or 5 min, respectively, were lysed in lysis buffer [for HEK-293 cells: 20 mM Tris·HCl, 150 mM NaCl, 10% glycerol, 5 mM EDTA, and 1% Nonidet P-40 complemented with proteinase and phosphatase inhibitors (Roche); for GCs: lysis buffer 9803 from Cell Signaling complemented with proteinase and phosphatase inhibitors (Roche)]. For immunoprecipitation, 400 μg of protein extract was incubated overnight at 4 °C with the antibody of interest. The mixtures were then incubated with protein G (GE Healthcare) or protein A/G Sepharose beads (Pierce) for 2 h at 4 °C. Sepharose beads were washed two times with 1% Nonidet P-40 buffer, one time with Tris·HCl buffer (20 mM Tris·HCl/150 mM NaCl, pH 7.5), and boiled in sample buffer before being subjected to SDS/PAGE analysis. Lysates were also separated on SDS/PAGE gels. SDS/PAGE gels were transferred on nitrocellulose membranes and immunoblotted. The following antibodies were used. For immunoprecipitation, mouse anti-Flk1 (recognizing the extracellular domain, AF644, 1/1,000; R&D Systems), mouse anti-NR2B (610416, 1/250; BD Biosciences), anti-phosphotyrosine PY99 (7020, 1/200; Santa Cruz Biotechnology), and mouse anti-phosphotyrosine 4G10 (1/100; Upstate) were used. As controls, mouse IgGs (Sigma) and rabbit IgGs (Sigma) were used. For immunoblotting, rabbit anti-Flk1 (recognizing the intracellular domain, 504, 1/200; Santa Cruz Biotechnology), mouse anti-Flk1 (recognizing the extracellular domain, AF644, 1/1,000; R&D Systems), mouse anti-Flk1 (6251, 1/100; Santa Cruz Biotechnology), rabbit anti-Flk1 (315, 1/100; Santa Cruz Biotechnology), rabbit anti-phospho-Flk1 Tyr^{951} (antibody against human Flk1 Tyr^{951} that cross-reacts with mouse Flk1-Tyr^{949} 4991, 1/1,000; Cell Signaling), rabbit anti-phospho-Flk1 Tyr^{1173} (2478, 1/1,000; Cell Signaling), rabbit anti-Src (05-184, 1/1,000; Millipore or sc-18, 1/1,000; Santa Cruz Biotechnology), rabbit anti–phospho-Src Tyr^{416} (2101, 1/1,000; Cell Signaling), mouse anti-NR2B (610416, 1/250; BD Biosciences), rabbit anti-NR2B (1557P, 1/1,000; Millipore), and mouse anti-NR1 (556308, 1/500; BD Biosciences) were used.

Analysis of Flk1 and NR2B Cell Surface Expression in Growth Cones. Heparin beads (H5263; Sigma) were extensively washed in PBS and soaked at room temperature for 4 h in PBS/BSA (0.5%), containing human $VEGF^{165}$ (50 mg/mL; R&D Systems) or control solution (0.5% PBS/BSA). After overnight incubation at 4 °C and subsequent rinses in PBS, control or VEGF-coated beads were inserted in plasma clots on poly-L-lysine/laminin-coated coverslips, onto which purified GCs were also plated and cultured in serum-free DMEM supplemented with N2 and B27. Plated GCs were then cultured in the presence of control or VEGF-coated beads for 16 h (to allow release of VEGF). Afterward, cultured GCs were fixed and processed for surface Flk1 and NR2B immunostaining as described above. Images of immunostained growth cones were acquired with an ApoTome microscope with a 63×/1.4 oil objective. Optical sections were imaged with an interval of 0.25 μm. Stacks of optical slices were collected digitally, after which 3D reconstructions were generated by using the Image J software. The total surface Flk1 and NR2B fluorescent area was measured by using the Image J software, keeping the same fluorescence intensity thresholds for each condition; these areas were then divided by the area of the growth cone. Colocalization of Flk1 and NR2B was assessed by using Image J and the "intensity correlation analysis" plug-in, as previously described (8). The area of colocalized pixels was then normalized to the total Flk1 or NR2B surface fluorescence.

1. Wirkner K, et al. (2007) Modulation of NMDA receptor current in layer V pyramidal neurons of the rat prefrontal cortex by P2Y receptor activation. *Cereb Cortex* 17: 621–631.
2. Du XL, et al. (2004) Differential effects of tyrosine kinase inhibitors on volume-sensitive chloride current in human atrial myocytes: Evidence for dual regulation by Src and EGFR kinases. *J Gen Physiol* 123:427–439.
3. Hatten ME (1985) Neuronal regulation of astroglial morphology and proliferation in vitro. *J Cell Biol* 100:384–396.
4. Borghesani PR, et al. (2002) BDNF stimulates migration of cerebellar granule cells. *Development* 129:1435–1442.
5. Renaud J, et al. (2008) Plexin-A2 and its ligand, Sema6A, control nucleus-centrosome coupling in migrating granule cells. *Nat Neurosci* 11:440–449.
6. Salin PA, Malenka RC, Nicoll RA (1996) Cyclic AMP mediates a presynaptic form of LTP at cerebellar parallel fiber synapses. *Neuron* 16:797–803.
7. Farrant M, Feldmeyer D, Takahashi T, Cull-Candy SG (1994) NMDA-receptor channel diversity in the developing cerebellum. *Nature* 368:335–339.
8. Li Q, et al. (2004) A syntaxin 1, $G\alpha_o$, and N-type calcium channel complex at a presynaptic nerve terminal: Analysis by quantitative immunocolocalization. *J Neurosci* 24:4070–4081.

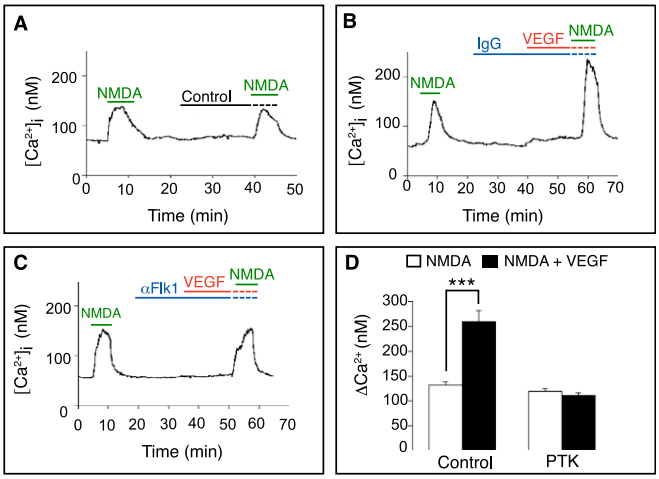

Fig. S1. VEGF enhances NMDA-stimulated $[Ca^{2+}]_i$ via Flk1 in GCs. (*A*) Representative single GC tracing of intracellular $[Ca^{2+}]_i$ levels obtained by Ca^{2+} imaging. GCs were stimulated a first time with NMDA, thereafter exposed to control buffer, and stimulated a second time with NMDA, revealing that control vehicle did not amplify the second NMDA response. (*B* and *C*) Single GC tracing of $[Ca^{2+}]_i$, showing abrogation of the increase in $[Ca^{2+}]_i$ by αFlk1 (*C*) but not by control IgG (*B*). (*D*) Measurements of ΔCa^{2+}, revealing inhibition of VEGF-dependent increase in $[Ca^{2+}]_i$ by PTK but not by control vehicle ($n = 164$, $^{***}P < 0.001$ for vehicle; $n = 142$, P = not significant for PTK).

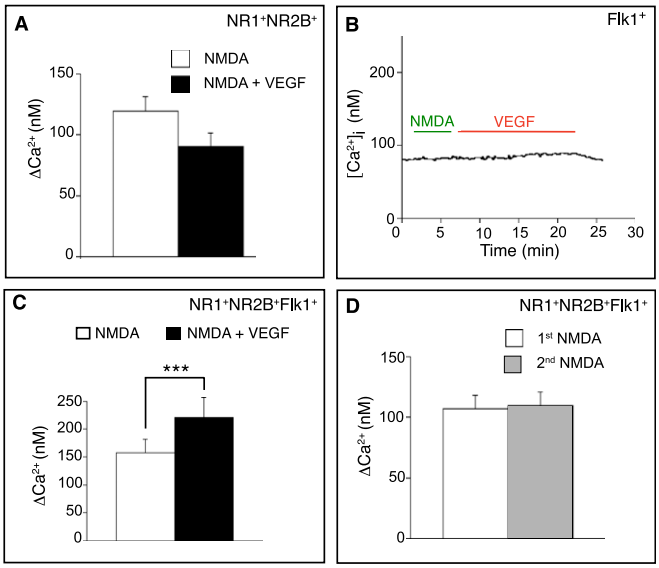

Fig. S2. VEGF potentiates NMDAR-mediated $[Ca^{2+}]_i$ in HEK-293 cells. (*A*) Measurements of ΔCa^{2+} revealing lack of VEGF-induced potentiation in HEK-293 cells cotransfected only with NR1 and NR2B (n = 79, P = not significant). (*B*) Representative $[Ca^{2+}]_i$ tracing of a single HEK-293 cell, transfected only with Flk1, revealing that VEGF itself did not elevate $[Ca^{2+}]_i$. (*C* and *D*) Measurements of ΔCa^{2+} in HEK-293 cells cotransfected with Flk1, NR1, and NR2B, showing that ΔCa^{2+} is increased by VEGF (n = 21, ***$P < 0.001$; *C*) but not by control vehicle (n = 16, P = not significant; *D*).

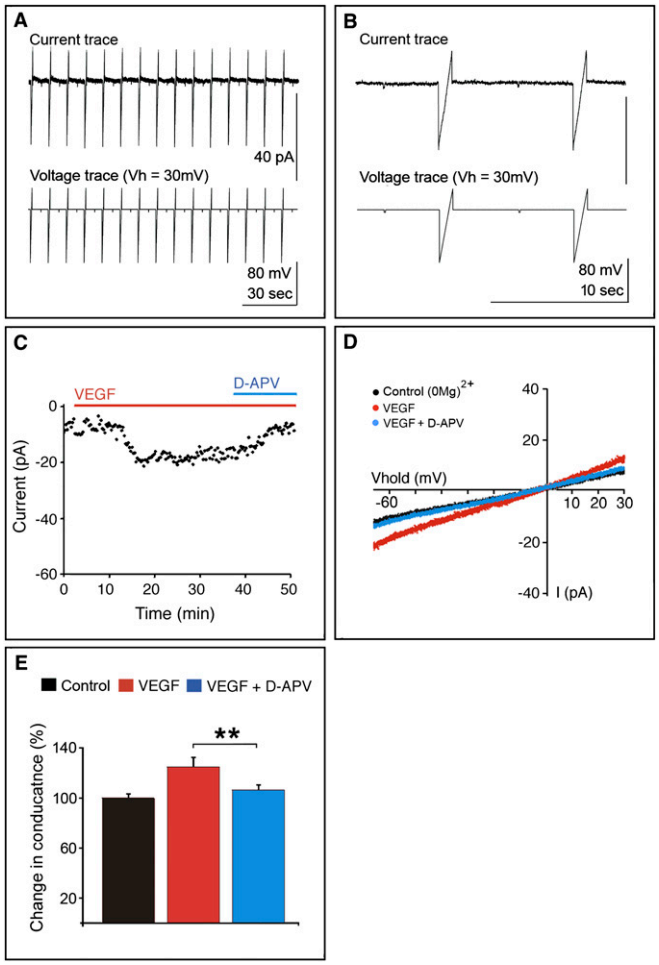

Fig. S3. VEGF induces small inward currents in GCs. (*A*) Representative current and voltage traces of a whole-cell patch–clamp recording of a GC in the lower EGL, showing no spontaneous synaptic events. (*B*) High magnification of the traces shown in *A*, illustrating the lack of synaptic events and the voltage ramp and square pulses. (*C*) Representative time course of whole-cell responses of a GC in the lower EGL, revealing a small inward current upon VEGF application, which was blocked by D-APV. (*D*) Current–voltage relationship of the responses of the GC shown in *C*, showing the inward current in response to VEGF alone, which was further blocked by D-APV. (*E*) Representation of the small changes in conductance after VEGF and VEGF + D-APV application, suggesting that most of the VEGF-induced current resulted from an amplification by VEGF of the NMDAR response to ambient glutamate in slices ($n = 7$, $^{**}P < 0.01$).

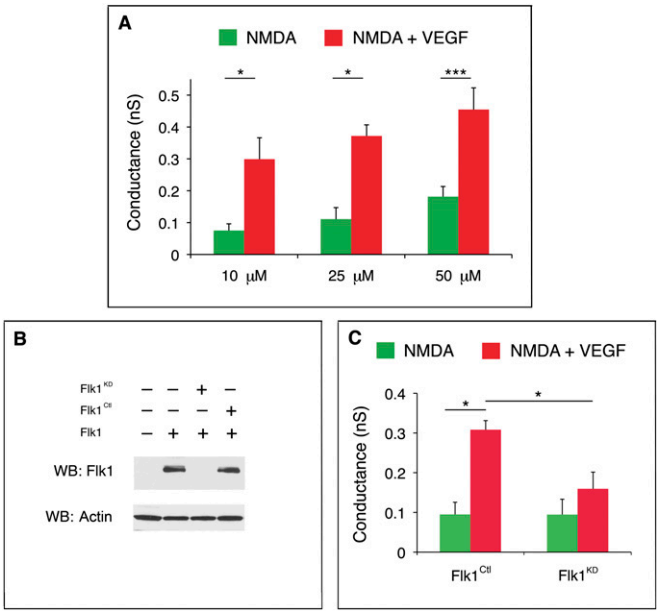

Fig. S4. Flk1 regulates VEGF-mediated potentiation of NMDAR currents in GCs. (*A*) VEGF potentiates NMDAR conductance induced at different concentrations of NMDA [n = 6, 7, and 26 at 10, 25, and 50 μM NMDA, respectively; $*P < 0.05$ and $***P < 0.001$ in VEGF + NMDA (red bars) versus NMDA (green bars)]. (*B*) Western blot showing down-regulation of Flk1 expression in HEK-293 cells cotransfected with Flk1 plus a shRNA construct for Flk1 ($Flk1^{KD}$) but not in HEK-293 cells transfected with Flk1 alone or cotransfected with Flk1 plus a control shRNA ($Flk1^{Ctl}$). (*C*) $Flk1^{Ctl}$ or $Flk1^{KD}$ constructs were coelectroporated with an EGFP expression vector in cerebella, and organotypic slices were cultured for 3 d before recording $EGFP^+$ GCs. Similar to results in acute slices, the NMDAR whole-cell patch-clamp conductance of $EGFP^+/Flk1^{Ctr}$ GCs in electroporated organotypic slices was increased after application of VEGF plus NMDA (red bar) compared with NMDA alone (green bar) (n = 5, $*P < 0.05$ in VEGF + NMDA versus NMDA for $Flk1^{Ctl}$ GCs). In contrast, Flk1 silencing in $EGFP^+/Flk1^{KD}$ GCs largely reduced the potentiating effect of VEGF on NMDAR-mediated currents (n = 5; $*P < 0.05$ for VEGF + NMDA in $Flk1^{KD}$ GCs versus VEGF + NMDA in $Flk1^{Ctl}$ GCs; P = not significant for NMDA versus NMDA + VEGF in $Flk1^{KD}$ GCs).

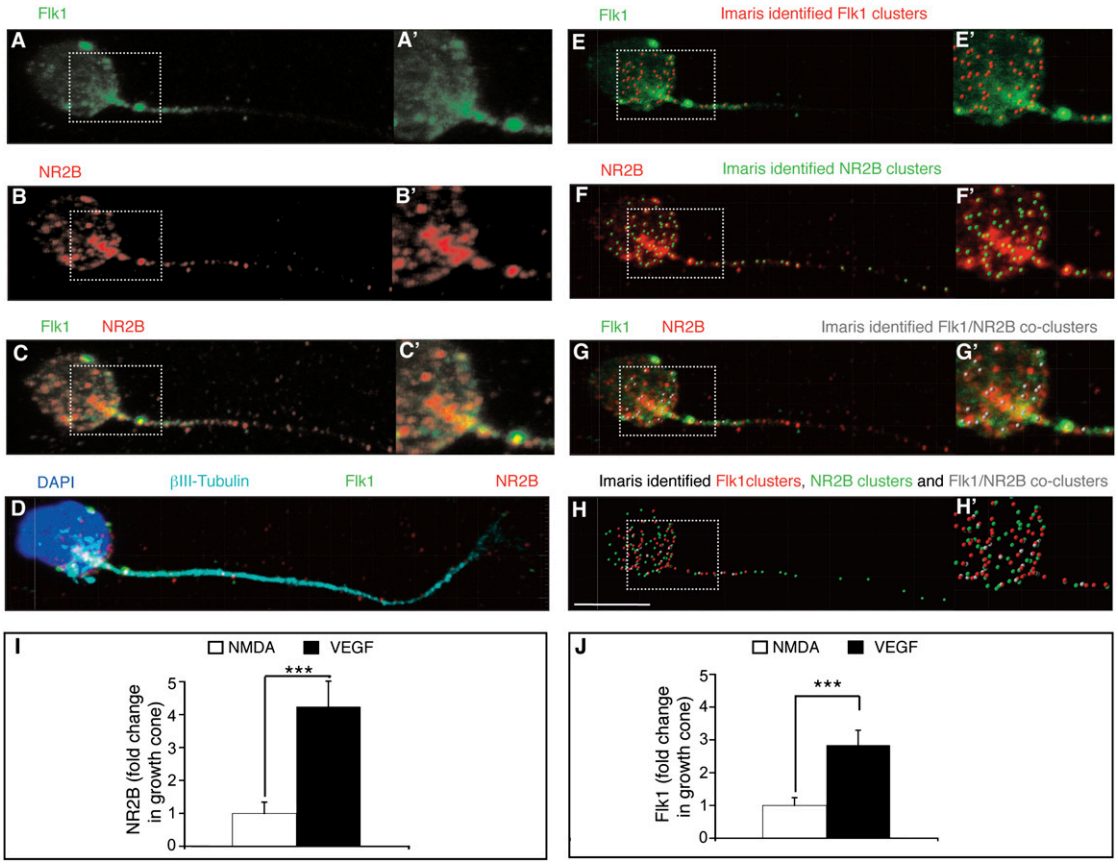

Fig. S5. VEGF induces coclustering of Flk1 and NR2B in GCs. (*A–D*) Maximum projection of 3D confocal *z*-stack images of a VEGF-treated GC immunostained for surface Flk1 (*A*, *C*, and *D*), NR2B (*B–D*), and β-III tubulin (*D*) and DAPI (*D*), revealing Flk1, NR2B, and Flk1/NR2B coclusters after VEGF stimulation. (*E–G*) Same images as in *A–C*, but now indicating the Imaris-detected clusters of Flk1 (red dots in *E* and *G*), NR2B (green dots in *F* and *G*), and Flk1/NR2B coclusters (white dots in *G*). (*H*) Representation of all Flk1 clusters (red dots), NR2B clusters (green dots), and Flk1/NR2B coclusters (white dots) identified by Imaris in the VEGF-treated GC shown in *A–D*. Insets *A′–C′* and *E′–H′* show a higher magnification of the area delineated by the white dashed box in the corresponding images. Clusters on the maximum projection of 3D confocal *z*-stack images were detected with the image analysis software package Imaris (version 6.3.1) by using a customized algorithm in which, for each fluorescent channel, a cluster was defined by an estimated diameter (between 0.04 and 0.1 μm) and by a threshold of mean fluorescence intensity (after subtraction of the background signal). Coclusters were identified by generating a colocalization channel, applying the same fluorescence intensity threshold and estimated diameter used for identifying single clusters. Note that the images showing the clusters in *E–H* were also generated by maximum projection of 3D confocal *z*-stack images. (*I* and *J*) Quantification of the cell surface NR2B fluorescence (*I*) and Flk1 fluorescence (*J*) in GC growth cones, revealing that exposure to VEGF increased the cell surface levels of both NR2B and Flk1 ($n = 25–19$ for NR2B, $^{***}P < 0.001$; $n = 25–19$ for Flk1, $^{***}P < 0.001$). (Scale bar: *A–H*, 5 μm.)

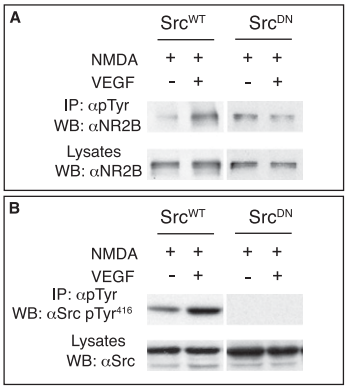

Fig. S6. VEGF induces NR2B phosphorylation via SFKs in the presence of NMDA. (*A* and *B*) HEK-293 cells were cotransfected with NR1, NR2B, Flk1, and Src^{WT} or Src^{DN}. At 24 h after transfection, cells were first stimulated with NMDA for 10 min and then stimulated with VEGF for 30 min in the presence of NMDA. Tyrosine phosphorylated proteins were immunoprecipitated with an anti-phosphorylated tyrosine (αpTyr) antibody and then immunoblotted with an anti-NR2B antibody (*A*) or an antibody against SFK-pTyr^{416} (αSFK-pTyr^{416}) (*B*), revealing that VEGF increased tyrosine phosphorylation of NR2B and Src in the presence of only Src^{WT} but not Src^{DN}. As loading controls, lysates were also immunoblotted for total NR2B (*A*) and Src (αSrc) (*B*).

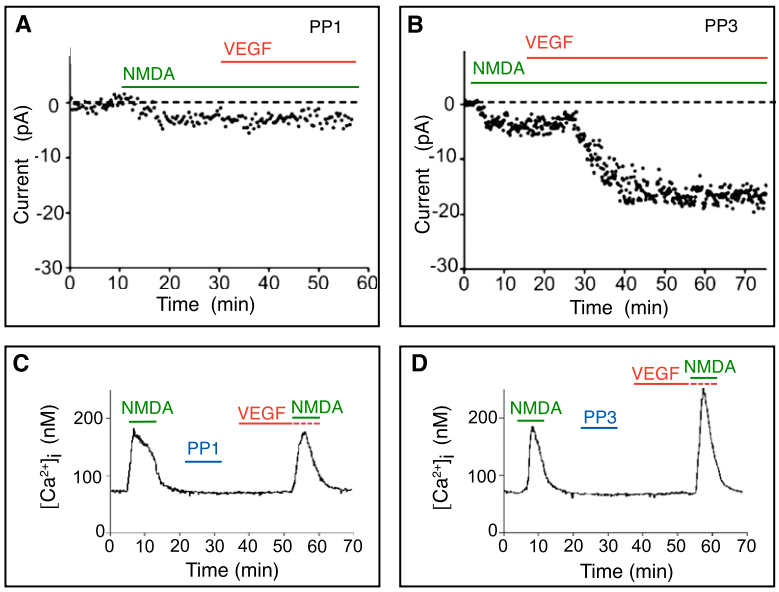

Fig. S7. VEGF-mediated potentiation of NMDAR activity requires SFK in GCs. (*A* and *B*) Representative whole-cell patch–clamp recording of a GC in the lower EGL, revealing inhibition of the VEGF-stimulated increase in NMDAR-mediated current by PP1 (*A*) but not by its inactive analog PP3 (*B*). (*C* and *D*) Representative $[Ca^{2+}]_i$ recording in a single GC, stimulated sequentially with NMDA, PP3 (*D*), or PP1 (*C*) for 10 min; with VEGF; and thereafter with NMDA, showing that PP1 blocked the VEGF-amplification of the NMDA response. Delivery of PP1 and PP3 was done as described by intracellular application in GCs in slices (1) or superfused in GC cultures (2).

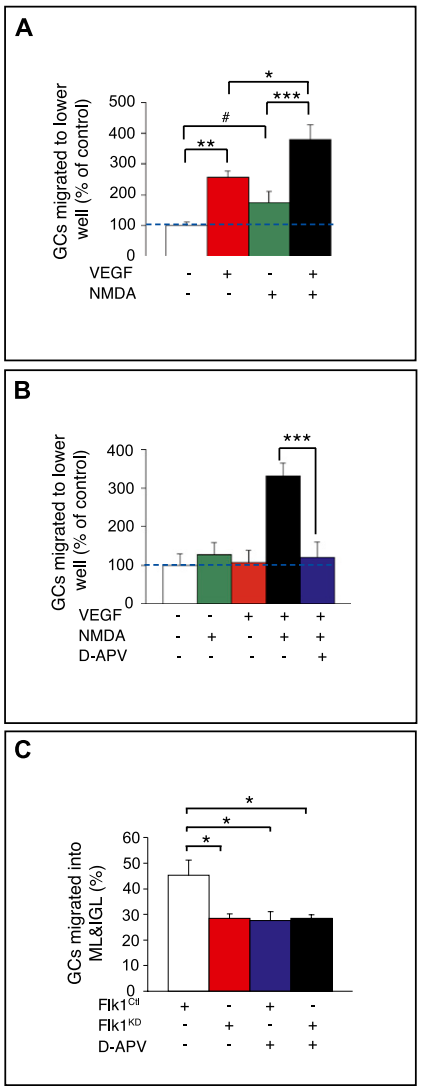

Fig. S8. VEGF plus NMDA stimulates GC migration. (*A* and *B*) Boyden chamber assay, illustrating the stimulatory effect of VEGF on NMDAR-dependent motility. (*A*) When VEGF is added to the lower chamber (red bar), GC migration was stimulated compared with the control (white bar). In contrast, when NMDA (10 μM) was added to the upper chamber (green bar), GC migration was not affected. The combination of VEGF in the lower chamber plus NMDA in the upper chamber increased GC migration (black bar) (*$P < 0.05$; **$P < 0.01$; ***$P < 0.001$; $^{\#}$Not significant). (*B*) Neither VEGF (red bar) nor NMDA (green bar) stimulated GC motility when added alone in the upper chamber. In contrast, when both VEGF and NMDA were added to the upper chamber (black bar), the resulting potentiation of GC chemokinesis was blocked by D-APV (***$P < 0.001$; blue bar), indicating that the effect of VEGF is mediated through NMDAR ($n = 7$). (*C*) Analysis of GC migration in organotypic cerebellar slices [expressed as percentage of $EGFP^+$ GCs in the molecular layer (ML) and internal GC layer (IGL) versus total number of $EGFP^+$ GCs in EGL, ML, and IGL], showing inhibition of GC migration upon knockdown of Flk1 ($Flk1^{KD}$, red bar) and upon blockage of NMDAR activity by D-APV treatment (blue bar). The combination of $Flk1^{KD}$ and D-APV did not reduce GC migration any further (black bar) (*$P = 0.01$), indicating that VEGF regulates GC migration via the aforementioned VEGF/NMDAR modulation.